Impact of Simulated M9 Cascadia Subduction Zone Motions on Base Isolated Structures

Tianye Yang[1], Nasser A. Marafi[2], Paolo M. Calvi[3],

Richard Wiebe[3], Marc O. Eberhard[4], Jeffery W. Berman[4]

[1]Ph.D. Student, Department of Civil and Environmental Engineering, University of Washington, Seattle, USA
[2]Postdoctoral Researcher, Department of Civil and Environmental Engineering, University of Washington, Seattle, USA
[3]Assistant Professor, Department of Civil and Environmental Engineering, University of Washington, Seattle, USA
[4]Professor, Department of Civil and Environmental Engineering, University of Washington, Seattle, USA

ABSTRACT

Engineers commonly use isolation systems to mitigate the effects of strong ground-shaking on super-structure responses, however, the behavior of such systems located in deep basin during an M9 earthquake is unknown. This paper studies the effects of an M9 CSZ earthquake on base-isolated systems using SDOF nonlinear time history analyses (NLTHA). The effects of simulated M9 motions on such systems were examined for both the Friction Pendulum System (FPS) and Double Concave Friction Pendulum (DCFP). The hysteretic behavior of an FPS and DCFP system had effective periods ranging from 1.5 to 5.0 seconds. Structures designed based on the NEHRP (2015) risk-targeted Maximum Considered Event (MCE_R) or the uniform hazard spectrum without considering the effects of the basin, resulted in displacement demands during the simulated M9 earthquake that, on average, exceeded the demands predicted using the design spectra. However, base-isolated systems that considered basin effects were found to have M9 CSZ displacement demands that did not exceed the design spectra, and can effectively protect the structure against the effects of the M9-induced shaking.

Keywords: Cascadia subduction zone, basin effect, ground motion, base isolation, friction pendulum systems

INTRODUCTION AND MOTIVATION

Based on geological evidence, the Cascadia Subduction Zone (CSZ) is capable of generating megathrust earthquakes up to magnitude 9 (M9) that may severely hit the Pacific Northwest (PNW) in the United States. In addition, many cities in the Pacific Northwest are underlain by a deep sedimentary basin that is known to amplify ground-motion intensity [1].

The results obtained from numerical simulations indicated that this type of earthquake may be particularly detrimental for structures characterized by fundamental period of vibration of 1.0 second or larger [2]. More specifically, the results of analyses conducted on a large set of single-degree-of-freedom (SDOF) structures with various combinations of strength and ductility subjected to the simulated M9 motions, showed that the deformation demands and the collapse likelihood for "flexible" (i.e. long period) structures are significantly larger than those obtained considering a "traditional" risk-targeted maximum considered event (MCE_R) that do not consider the effects of the basin.

This finding may be particularly relevant for base isolated structures. Base isolation systems are often used to control the displacement and acceleration response of the superstructure, and thus mitigate the damage caused by the strong motions. Base isolated structures tend to be characterized by effective period of vibration larger than 1.0 second. However, this type of systems have not been included in the studies conducted thus far, and the effects of the M9 earthquake on their performance and vulnerability remain unclear.

To provide insight into the response of base isolated structures to the simulated M9 earthquakes, this paper presents the results of nonlinear time history analysis (NLTHA) conducted on a large set of SDOF systems that represent the hysteretic behavior of FPS and DCFP characterized by effective periods ranging from 1.5 to 5 seconds. A state-of-the-art review on the development and behavior of friction type base isolation systems can be found in [3]. These SDOF structures were designed based on either code-required design spectra or modified design spectra for MCE_R hazard level for downtown Seattle area based on previous studies, in particular, the following four spectra were chosen for this study.

- MCE$_R$ design spectrum based on NEHRP 2015 [4], denoted as MCE$_R$, which does not account for the basin.
- Uniform hazard spectrum without any basin amplification factors (computed using the USGS NSHMP Code 2018 [5]), denoted as UHS.
- Uniform hazard spectrum with Campbell and Bozorgnia [6] basin amplification factors (calculated assuming $Z_{2.5} = 7$ km), denoted as UHS CB14.
- Uniform hazard spectrum with M9 basin amplification factor [2], denoted at UHS M9 BAF.

Figure 1 shows the response spectra for the four design spectra considered in this study. It should be noted that the basin effects mainly affect spectral accelerations at long periods (>1s).

The main goal of this study is to evaluate the performance of the friction type bearings, in particular, FPS and DCFP, during an M9 earthquake, when designed based on the above four response spectra. Maximum displacement is chosen as the parameter of interest for this study as it is the engineering demand parameter that is most directly related to the failure of base isolation systems and its strong correlation to the maximum base shear.

DESIGN SPECTRA

The risk-targeted maximum considered earthquake spectra (shown as a solid black line in Figure 1) is used to estimate the seismic demands of most structures in the US [4]. However, this MCE$_R$ spectra is only an approximation of the uniform hazard spectra (UHS) and only matches the uniform hazard at two periods (0.2 s and 1.0 s). While this approximation is considered sufficient for most structural applications, engineers typically use the uniform hazard spectra (shown as a solid grey line in Figure 1) to design and evaluate base isolation systems.

Additionally, the uniform hazard spectra in areas located on deep basins is under predicted because basin effects are not currently considered in the probabilistic seismic hazard code [5] used to generate the national seismic hazard maps used in ASCE 7-16 [7]. Engineers in the Seattle region have recognized this deficiency [8] in the seismic hazard and have amplified the UHS using basin amplification factors (dashed grey line shown in Figure 1). These basin amplification factors were computed using the Campbell and Bozorgnia [6] ground motion model and were derived from basins in California subjected to crustal earthquakes.

More recently, Marafi et al. [9] have shown that deep basins in subduction regions have different basin amplification factors than those derived from basin regions with crustal earthquakes. Frankel et al. [1] used physics-based ground motion simulations to predict amplification factors in the basins surrounding the Puget Sound region during a magnitude-9 subduction earthquake from the Cascadia Subduction zone. These amplification factors (computed in [2]) are also considered here and are shown in Figure 1 (dashed dot-line). This paper designs base isolators which consider each of the four design spectra, separately (shown in Figure 1). The performance of base isolators considering each of the four design spectra variations are later compared.
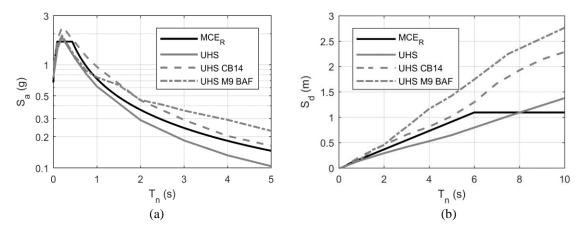

Figure 1. The (a) design spectral accelerations and (b) design spectral displacements with respect to the fundamental period of the structure (T_n) for the risk-adjusted maximum considered earthquakes (MCE$_R$), uniform hazard spectra (UHS), uniform hazard spectra with CB14 basin amplification factors (UHS CB14), and uniform hazard spectra with basin amplification factors derived from the M9 CSZ simulations (UHS M9 BAF).

NUMERICAL ANALYSIS

Ground Motion Selection and Scaling

The performance of the base isolation systems at multiple periods was assessed using motions that were scaled and selected to match the four design spectra variations and later compared to ground-motions from the suite of M9 CSZ scenarios in Seattle. The seismic hazard in the Pacific Northwest is controlled from both crustal and subduction zone earthquakes sources. Therefore, for each design spectra, 60 ground motions were selected from recorded crustal earthquakes in the NGA-West-2 database [10], and another 60 ground motions were selected from recorded subduction zone earthquakes from the KiK-Net/K-Net database [11].

For crustal earthquake motions matched to the each design spectrum, 60 ground motions were selected and scaled from the NGA-West-2 strong motion database that were the most spectrally equivalent to the design spectra. In addition, ground motions were selected to have: (1) a unscaled peak ground acceleration of at least 0.05g, (2) a source-to-site (Joyner-Boore) distance between 5 to 100 km, (3) a significant duration ($D_{s,5-95}$) between 1 to 60 seconds, and (4) did not include any pulse-like characteristics.

To select the most spectrally-equivalent ground motions, each ground motion in the database was scaled to have a minimum 2-norm log-scale error to the design spectrum for periods between 1 to 6 seconds. This period range was chosen because it often characterizes the equivalent natural period of a base isolated system. For each design spectra, 60 ground motions with the least 2-norm log-scale errors were selected with scale factors restricted to be between 0.2 and 5.

A similar ground-motion scaling approach was used for subduction zone earthquakes. However, these records were only selected (1) from either the 2001 M_w8.3 Tokachi-Oki earthquake, 2011 M_w 9.0 Tohoku earthquake, and 2011 M_w 7.9 Tohoku aftershock earthquakes, and (2) had an unscaled peak ground acceleration of at least 0.05g. As an example, Figure 2 shows the median of the scaled selected ground motion acceleration spectra for crustal and subduction zone ground motions scaled and selected to the (a) MCE_R, and (b) to the UHS with basin amplification factors derived from the suite of M9 CSZ simulations.
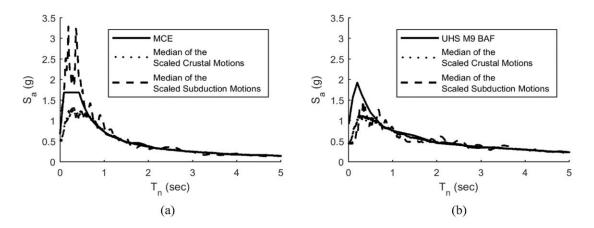

Figure 2. Acceleration spectra comparison between (a) MCE; (b) UHS M9 BAF and the corresponding scaled ground motions from NGA-WEST2 (crustal) and the subduction zone ground motion database.

Base Isolation Design

The design of the SDOF structures representing the studied friction pendulum systems follows a Direct Displacement Based Design procedure (DDBD). The procedure of applying DDBD on friction type base isolation systems can be found in [12]. In [12], the isolation system and the base shear demand for the superstructure were designed given a designed displacement value and an α value (which equals to the ratio between the maximum designed based shear and the force required to activate the slider). This design procedure was modified in this study such that the isolation system and the base shear demand value were designed given a target effective period, T_{eff}, and an α value, which is summarized as follows.

Given an α value, the equivalent damping ratio, ζ, is calculated using Eq. (1), where the derivation can be found in [12]. Then a displacement reduction factor, η, calculated using Eq. (2) [13], is applied to the design displacement spectrum. The displacement demand, Δ_d, of the isolator is obtained from the reduced displacement spectrum with the corresponding designed effective period value.

$$\zeta = \sqrt{2/\pi\alpha} \tag{1}$$

$$\eta = \sqrt{7/(2 + \zeta)} \tag{2}$$

With the effective period, the effective stiffness, K_{eff}, of the isolation system is calculated using Eq. (3), where m represents the total mass of the superstructure. Then the base shear demand for the superstructure, V_{max}, is simply obtained using Eq. (4).

$$K_{eff} = 4\pi m^2 / T_{eff}^2 \tag{3}$$

$$V_{max} = K_{eff} \cdot \Delta_d \tag{4}$$

Once the shear demand is calculated, the bearing properties, including the effective radius of curvature, R_{eff}, and the coefficient of friction between the slider and the concave sliding surface, μ, can be determined using Eq, (5) and Eq. (6), respectively.

$$\mu = V_{max}/\alpha m g \tag{5}$$

$$R_{eff} = mg\Delta_d / (V_{max} - V_{max}/\alpha) \tag{6}$$

The α value used in this design procedure is chosen by the design engineer. For a fixed design effective period, as the α value increases, the effective damping decreases, resulting in a greater displacement reduction factor. Effectively, increasing in α value will increase the displacement demand. Based on Equation (4) to Equation (6), an increased α value would also decrease both the effective radius of curvature and coefficient of friction.

To achieve practical values for both the effective radius of curvature and coefficient of friction, α values usually range from 2.5 to 4.5. To keep the consistency in this study, an α value of 3 was used throughout the design. The final properties for the FPS and DCFP designed for this study are summarized in Table 1. For each design spectrum, base isolators with effective fundamental periods ranging from 1.5 seconds to 5 seconds (with an increment of 0.5 seconds) were designed. It is worth mentioning that common DCFP systems have symmetric geometric and frictional properties. Such systems, when having half the effective radius of curvature with the same frictional properties compared to FPS, it yields almost identical hysteretic behavior as the corresponding FPS [14]. Thus only the design properties for the FPS are listed.

Table 1. Design properties of the FPS

T_{eff} (sec)	MCE			UHS			UHS CB14			UHS M9 BAF		
	R (m)	μ (%)	Δ_d (m)	R (m)	μ (%)	Δ_d (m)	R (m)	μ (%)	Δ_d (m)	R (m)	μ (%)	Δ_d (m)
1.5	0.84	9.0	0.15	0.84	8.3	0.14	0.84	12.9	0.22	0.84	11.7	0.20
2.0	1.49	6.7	0.20	1.49	5.3	0.16	1.49	8.3	0.25	1.49	8.4	0.25
2.5	2.33	5.4	0.25	2.33	4.4	0.20	2.33	6.8	0.32	2.33	7.5	0.35
3.0	3.35	4.5	0.30	3.35	3.4	0.23	3.35	5.4	0.36	3.35	6.6	0.45
3.5	4.57	3.8	0.35	4.57	2.9	0.27	4.57	4.6	0.42	4.57	6.0	0.55
4.0	5.96	3.4	0.40	5.96	2.4	0.29	5.96	3.7	0.45	5.96	5.4	0.64
4.5	7.55	3.0	0.45	7.55	2.2	0.33	7.55	3.4	0.51	7.55	4.8	0.72
5.0	9.32	2.7	0.50	9.32	2.0	0.35	9.32	3.0	0.56	9.32	4.2	0.78

Analysis Procedure

Four groups of NLTHA were performed, each one corresponding to one design spectrum mentioned in Section "Design Spectra".

The bearings designed for each spectrum are summarized in Table 1, and their hysteretic behavior were represented using SDOF systems. Nonlinear time history analyses were performed in OpenSees [15], in which the friction pendulums were modeled using the Single Friction Pendulum Bearing Element [16].

For each SDOF structure, the following three sets of ground motions were considered for the NLTHA, and the maximum absolute displacements from the analyses were recorded.

- 60 scaled ground motions selected and scaled from NGA-West-2 database.
- 60 scaled ground motions selected and scaled from the subduction zone ground motion database.
- 30 pairs of the simulated M9 motions.

It should be noted that all of the analyses are performed such that the structure was under uni-directional shaking, however, the simulated M9 motions are given in orthogonal pairs. To compare the maximum displacement among each group in a fair manner, the geometric mean of the resulting responses from the paired M9 motions were compared with the maximum displacements from the two other groups.

NUMERICAL ANALYSIS RESULTS

For each design spectrum, the design displacement versus the effective period were plotted. These values directly come from the reduced displacement spectrum as mentioned in the DDBD procedure. Then the median maximum displacements for each effective period from each NLTHA group were plotted. As mentioned in the introduction section, the return period of the M9 earthquake is approximately 500 years; the 84th percentile of the maximum displacements from the M9 motions would be corresponding to a return period that is approximately 2500 years, which is the return period of the MCE hazard level. To indicate the extreme case from M9 motions, the 100th percentile of the maximum displacements for each effective period was also plotted.

For brevity, only the results for MCE and UHS with M9 BAF are presented here. The UHS without any basin amplification factors yielded similar results as the MCE group, and the UHS with CB14 amplification factors yielded similar results as the UHS with M9 BAF group.

First, as shown in Figure 3, the median maximum displacement responses from both spectrum-matching motions selected from crustal motions and subduction zone motions match well with the design displacement demands. This indicates that the DDBD procedure and the ground motion selection and scaling procedure adopted in this study provided good preliminary approximation on the maximum displacement compared to the NLTHA results.
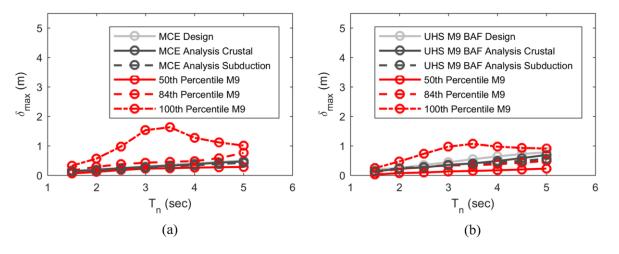

Figure 3. Design period versus maximum displacement for (a) MCE; (b) UHS with M9 BAF.

Secondly, the median response (i.e. 50th percentile M9 as shown in Figure 3) from the simulated M9 motions falls below the design displacement demands by an average value of approximately 10% for the considered period range (for all four considered design spectra). However, when comparing the response with compatible return periods (i.e. 84th percentile maximum displacement from simulated M9) with the design displacement demands based on MCE or UHS without basin amplification factors, the 84th percentile maximum displacement responses from the simulated M9 motions have displacement demands increase of 1%, 8.6%, 12.6%, 12.6%, 10.5%, 8%, 12.9%, 26%, and 4%, 20%, 25.2%, 27.5%, 28.2%, 33.7%, 34.7%, 52.3%, respectively, for periods ranging from 1.5 to 5 seconds with an increment of 0.5 seconds.

In contrast, when designed based on UHS with CB14 amplification factors, the 84th percentile curve from M9 is approximately on top of the design displacement curve. When designed with UHS with M9 BAF, the 84th percentile curve from M9 falls below the design displacement curve and have an average decrease of demands of 17.2%.

To analyze the results for each period in more detail, the probability of the maximum displacement exceeding certain displacement values for each period were plotted in Figure 4 and Figure 5 (again, the results for UHS without any basin amplification factors and for UHS with CB14 amplification factors are omitted as they, respectively, behave similarly to MCE and UHS with M9 BAF). It is shown that when the isolation systems are designed based on UHS with either CB14 or M9 amplification factors, the probability of the maximum displacement from the M9 motions exceeding certain displacement values are almost always lower than the probability of the maximum displacement from the design spectra-matching motions exceeding the same displacement values. However, when designed based on MCE or UHS without basin amplification factors, the probability of the maximum displacement from the M9 motions exceeding certain displacement values are sometimes higher than those obtained from the design spectra-matching motions, indicating the displacement demand obtained from the design spectra would not be able to perform well during the simulated M9 earthquake.

Finally, as shown in Figure 3, while the relationships between the displacement demand and the fundamental period for the design spectra are approximately linear, the 100th percentile maximum displacement from the simulated M9 motions indicates a particularly large displacement demand for effective periods between 2.5 to 4 seconds. This results match with what was found by Marafi et al. [2].

CONCLUSIONS

This study investigated the performance of base isolated structures, in particular, FPS and DCFP with symmetric geometric and frictional properties, under the effect of Cascadia Subduction Zone M9 earthquakes. A large set of SDOF structures were designed based on MCE$_R$ level design spectra and evaluated with the simulated physics-based simulated M9 motions. The considered design spectra includes risk-targeted MCE$_R$ design spectrum from NEHRP 2015, UHS without any basin amplification factors, UHS with CB14 amplification factors, and UHS with M9 basin amplification factors. It was found that, when comparing the 84th percentile maximum displacement values (which has approximately the same return period as the MCE level earthquakes) with the design displacement demands, the first two groups (without basin amplification factors) exceed the demands, and the last two groups (with basin amplification factors) did not. Within the 30 pairs of the simulated M9 motions, a small subset of the motions were found to be particularly damaging. The reasons requires further investigation.
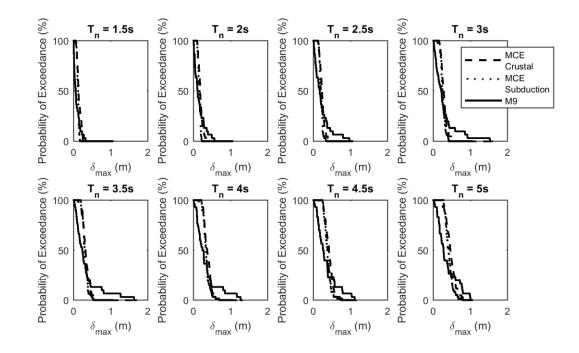
Figure 4. Probability of exceedance of the maximum displacement value for each design period using MCE spectrum
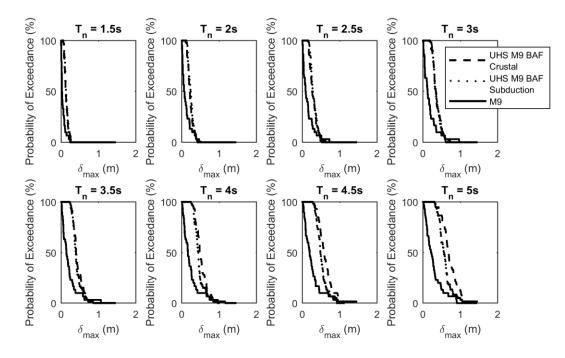

Figure 5. Probability of exceedance of the maximum displacement value for each design period using UHS M9 BAF

REFERENCES

[1] Frankel, A.D., Wirth, E.A., Marafi, N.A., Vidale, J., and Stephenson, W. (2018). "Broadband synthetic seismograms for Magnitude 9 earthquakes on the Cascadia megathrust based on a 3D simulations and stochastic synthetics, part 1: methodology and overall results". *Bulletin of the Seismological Society of America*, 108(5A), 2347-2369.

[2] Marafi, N.A., Eberhard M.O., Berman J.W., Wirth, E.A., Frankel, A.D. (2019). "Impacts of Simulated M9 Cascadia Subduction Zone Motions on Idealized Systems". *Earthquake Spectra. In press.*

[3] Calvi, P.M., and Calvi, G.M. (2018). "Historical development of friction based seismic isolation systems". *Soil Dynamics and Earthquake Engineering*, 106: 14-30.

[4] National Earthquake Hazards Reduction Program - NEHRP (2015). *NEHRP Recommended Seismic Provisions for New Buildings and Other Structures. 2015 Edition*. Prepared by FEMA, Washington, D.C., USA.

[5] USGS (United States Geological Survey), 2018. *"National Seismic Hazard Mapping Project (NSHMP) Code."* *https://github.com/usgs/nshmp-haz*.

[6] Campbell, K.W., and Bozorgnia, Y. (2014). "NGA-West2 ground motion model for the average horizontal components of PGA, PGV, and 5% damped linear acceleration response spectra". *Earthquake Spectra,* 30(3): 1087–1115.

[7] ASCE (2017). *Minimum Design Loads and Associated Criteria for Buildings and Other Structures*. ASCE/SEI 7-16. Reston, VA: American Society of Civil Engineering.

[8] Chang, S.W., Frankel, A.D., and Weaver, C.S. (2014). *Report on workshop to incorporate basin response in the design of tall buildings in the Puget Sound region, Washington. U.S*. Geological Survey, Open-File Report 2014-1196.

[9] Marafi, N.A., Eberhard, M.O., Berman, J.W., Wirth, E.A., and Frankel, A.D. (2017). "Effects of deep basins on structural collapse during large subduction earthquakes". *Earthquake Spectra,* 33(3): 963–997.

[10] Pacific Earthquake Engineering Research Center (2010). *Next Generation Attenuation (NGA) - West2*. https://peer.berkeley.edu/research/nga-west-2 (last accessed October 2018)

[11] K-NET and KiK-net strong-motion seismograph networks, 1996. http://www.kyoshin.bosai.go.jp/ (last accessed October 2018)

[12] Calvi, P.M., Moratti, M,, and Calvi, G.M. (2016). "Seismic isolation devices based on sliding between surfaces with variable friction coefficient". *Earthquake Spectra*, 32(4), 2291-2315.

[13] Priestley M.J.N., Calvi, G.M., Kowalsky, M.J. (2007). *Displacement based seismic design of structures*. IUSS Press, Pavia, Italy.

[14] Fenz, D.M., and Constantinou, M.C. (2006). "Behaviour of the double concave Friction Pendulum bearing". *Earthquake Engineering and Structural Dynamics*, 35(11), 1403-1424.

[15] Pacific Earthquake Engineering Research Center (2006). Open System for Earthquake Engineering Simulation (OpenSees) v.2.5.0. PEER, University of California, Berkeley, CA, USA. http://OpenSees.berkeley.edu.

[16] Mosqueda, G., Whittaker, A.S., and Fenves, G.L. (2004). "Characterization and modeling of friction pendulum bearings subjected to multiple component of excitation". *Journal of Structural Engineering*, 130(3), 433-442.